Radiation Physics and Chemistry 212 (2023) 111101

Contents lists available at ScienceDirect

Radiation Physics and Chemistry

journal homepage: www.elsevier.com/locate/radphyschem

^{76}Se(n,2n)^{75}Se reaction cross section measurement at 14.77 MeV neutron energy

T.S. Ganesapandy [a], G.T. Bholane [a], S.H. Patil [a], S.S. Dahiwale [a], S.G. Kulkarni [b], V.N. Bhoraskar [a], S.D. Dhole [a,*]

[a] Department of Physics, Savitribai Phule Pune University, Pune, 411007, India
[b] Department of Physics, Willingdon College, Sangli, 416415, India

ARTICLE INFO

Handling Editor: Dr. Chris Chantler

Keywords:
Neutron activation analysis
Nuclear reactions
Nuclear codes
Selenium-75
γ-ray spectrometry

ABSTRACT

The cross section of ^{76}Se(n,2n)^{75}Se reaction at 14.77 ± 0.17 MeV neutron energy was measured with offline gamma spectrometry. Furthermore, covariance analysis for the measured cross section with respect to the other neutron induced reaction cross sections for the same target was reported. The experimental results were compared with reported experimental data from the EXFOR database and evaluated data from the ENDF/B-VIII.0, JENDL-5, and TENDL-2021 libraries. Statistical model calculations with the TALYS-1.96, and EMPIRE-3.2.3 codes were carried out for optimized parameters corresponding to experimental trends. The measured cross section is in good agreement with the data from the EXFOR database, and the evaluated data libraries.

1. Introduction

Selenium (Se) is a grey non-metal found to occur in nature as seven stable isotopes. The isotopic abundance for ^{76}Se is 9.37 ± 0.29% in a natural Se sample. ^{75}Se decays by electron capture with a half-life 119.78 ± 0.05 days. The authors (Weeks and Schulz, 1986) explored the use of ^{75}Se as a potential gamma source as an alternative to iridium-192 for brachytherapy. The advantages of ^{75}Se as a source are the longer half-life, and the lower energy gamma rays. In literature, only a few previous works for the ^{76}Se(n,2n)^{75}Se reaction cross section have been reported in the experimental exchange format (EXFOR) database (Otuka et al., 2014). Only two of the reported experimental measurements are carried out with a high purity germanium (HPGe) detector and the sources of error in the experimental parameters are not adequately reported. In light of the various discrepancies in the previous reported data, the re-measurement of ^{76}Se(n,2n)^{75}Se reaction cross section is reported in the present work.

The article primarily reports and discusses the newly measured cross section of ^{76}Se(n,2n)^{75}Se reaction. Additionally, it presents other n+Se activation cross sections obtained in the same measurement and their correlations. This includes the description of the sample preparation, sample irradiation, induced activity measurement with γ-ray spectrometry, and uncertainty. In addition, statistical model calculations with the TALYS, and EMPIRE codes are done for the possible neutron-induced reactions on natural Se target. The measured cross sections are compared with the experimental data from literature and evaluated data from the ENDF database (Brown et al., 2018; Iwamoto et al., 2023; Koning et al., 2019).

2. Experimental methods

2.1. Sample activation and γ-ray spectrometry

Samples of selenium (Se) powder (99.99% purity) of natural isotopic abundance were prepared by packing ~2 gm sample in polythene vials. The samples were sandwiched between two aluminium (Al) foils weighing 0.285 gm in total and the sample size was 10 mm × 10 mm with a thickness 1 mm. The sample details are listed in Table 1. The samples were irradiated at the 14 MeV Neutron Generator facility (Bhoraskar, 1989), Department of Physics, Savitribai Phule Pune University, Pune, India. The 14 MeV neutron beam was produced by bombarding 150 ± 1 keV D^+ ions on an 8 Ci titanium-tritide solid target. The neutron energy at the sample position is 14.77 ± 0.17 MeV(Ganesapandy et al., 2023). The neutron flux during irradiation was found to be ~10^8 n/cm^2/s with Al foil activation. After irradiation for an hour, the samples were transferred to the counting room. After a sufficient cooling

* Corresponding author.
E-mail address: sanjay@physics.unipune.ac.in (S.D. Dhole).

https://doi.org/10.1016/j.radphyschem.2023.111101
Received 20 February 2023; Received in revised form 26 April 2023; Accepted 7 June 2023
Available online 8 June 2023

Table 1
Sample details.

Target isotope	Abundance (Meija et al., 2016) (%)	Sample weight (g)	Sample thickness (cm)	Sample density (g/cm^3)
^{82}Se	8.73 ± 0.22	2.0281 ± 0.005	0.1	4.81
^{80}Se	49.61 ± 0.41			
^{78}Se	23.77 ± 0.28			
^{77}Se	7.63 ± 0.16			
^{76}Se	9.37 ± 0.29			
^{74}Se	0.89 ± 0.04			
^{27}Al	100	0.2854 ± 0.0005	0.02	2.7

Table 2
Decay details for sample and reference monitor reactions.

Product Nuclei	Decay mode [a]	Half-life [b]	Eγ (keV)	Iγ (%)	Reference
^{81}Se^m	IT (99.949%)	57.28 ± 0.02 min	103.01	12.8 ± 0.3	Baglin (2008)
^{77}Ge	β$^-$ (100%)	11.211 ± 0.003 h	211.03	30.0 ± 0.8	Singh and Nica (2012)
^{78}As	β$^-$ (100%)	90.7 ± 0.2 min	694.9	16.7 ± 2.1	Farhan and Singh (2009)
^{75}Se	ec (100%)	119.78 ± 0.05 d	136	58.5 ± 0.4	Negret and Singh (2013)
^{76}As	β$^-$ (100%)	26.24 ± 0.09 h	559.1	45.0 ± 2.0	Singh (1995)
^{73}Se^g	ec β$^+$ (100%)	7.15 ± 0.09 h	361.2	97.0 ± 1.0	Singh and Chen (2019)
^{27}Mg	β$^-$ (100%)	9.458 ± 0.012 min	843.76	71.80 ±0.02	Shamsuzzoha Basunia (2011)
^{24}Na	β$^-$ (100%)	14.997 ± 0.012 h	1368.626	99.9936 ± 0.0015	Firestone (2007)

[a] IT → internal transistion, β$^-$ → Beta decay, ec → electron capture, β$^+$ → positron emission.
[b] min → minute, hr → hour, d → day.

time, the induced gamma activity of the irradiated samples was measured with a pre-calibrated lead-shielded Ortec HPGe detector having 30% relative efficiency and 1.5 keV energy resolution at 1.33 MeV gamma energy. The Ortec-make MCA and the MAESTRO software were used for the data acquisition. The decay details of the activated product nuclei, and references for the data analysis are provided in Table 2. The threshold energy, timing details and γ-ray net peak counts for the possible neutron-induced reactions on a selenium target are listed in Table 3. The recorded γ-ray spectra for irradiated Se sample and Al monitor are shown in Fig. 1 along with the respective irradiation time (t_1), cooling time (t_2) and counting time (t_3). In Fig. 1 (a) the short half-life gamma-ray spectrum is shown. In Fig. 1 (b) and (c), the long half-life gamma-ray spectra are shown for product nuclides ^{81}Se^m, ^{77}Ge, ^{78}As, ^{75}Se, ^{76}As and ^{73}Se^g along with the monitor reaction product nuclide ^{24}Na.

2.2. Detection efficiency determination of the HPGe detector

Standard point sources ^{152}Eu ($T_{1/2}$ = 13.517 ± 0.009 years and activity A_0 = 4336.98 ± 86.74 Bq as on 1 Oct. 1999), and ^{133}Ba ($T_{1/2}$ = 10.51 ± 0.05 years and activity A_0 = 37000 ± 140 Bq as on 1 Jan. 2019) were used to calibrate the HPGe detector at a distance 50 mm from the detector surface. The required efficiencies for sample geometry (ε) and sample position at 5 mm were transferred with the EFFTRAN code (Vidmar, 2005). The detection efficiency uncertainties were calculated by the method described in Ref. (Ganesapandy et al., 2022a). The following linear parametric model was used to generate the efficiencies that are listed in Table 4 at required energies of γ-lines in MeV

$$ln\,\varepsilon = -3.4025 - 0.914\ln E + 0.1729\ln E^2 + 0.4459\ln E^3 + 0.3273\ln E^4 + 0.0834\ln E^5 \quad (1)$$

2.3. Measurement of neutron-induced cross section and associated uncertainty

The cross section for the following reactions ^{82}Se(n,2n)^{81}Se^m, ^{80}Se(n,a)^{77}Ge, ^{78}Se(n,p)^{78}As, ^{76}Se(n,2n)^{75}Se, ^{76}Se(n,p)^{76}As, ^{74}Se(n,2n)^{73}Se^g were calculated with the ^{27}Al(n,a)^{24}Na reaction as the monitor reaction with the following expression:

$$\sigma_s = \sigma_m \frac{\varepsilon_m\, C_s\, a_m\, A_s\, M_m\, I_{\gamma m}\, f_m\, F_s}{\varepsilon_s\, C_m\, a_s\, A_m\, M_s\, I_{\gamma s}\, f_s\, F_m} \quad (2)$$

here, the sample reaction parameters and the monitor reaction parameters are referred to with the subscript s and m respectively. ε is the detector efficiency, C is the photo peak counts, a is the isotopic abundance, A is the atomic mass, M is the mass, $I\gamma$ is the branching ratio of γ-ray and f is the timing factor. The timing factor f is given by

$$f = \frac{(1 - e^{-\lambda t_1})(e^{-\lambda t_2})(1 - e^{-\lambda t_3})}{\lambda} \quad (3)$$

where, λ is the decay constant, t_1 is the irradiation time, t_2 is the cooling time and t_3 is the counting time. σ_m = 111.69 ± 2.73 mb is the interpolated IRDFF-II evaluated cross section at 14.77 ± 0.17 MeV for the ^{27}Al(n,α)^{24}Na reaction. The correction factor (F) due to the coincidence summing effects (f_c) and the gamma ray self-attenuation (f_a) is given by $F = f_c \times f_a$. f_c was calculated with the TrueCoinc code (Sudar, 2002). f_a was calculated with self-absorption coefficients retrieved from the XMuDat database(Pronyaev, 1998). f_c, f_a, and F for the product nuclides are listed in Table 5.

The fractional uncertainties in the measured parameters of equation (2) were propagated to σ_s following the Ref. (Ganesapandy et al., 2022b). The fractional uncertainties *As*, *Am* and *am* are negligible. $\eta_{m,s} = \frac{\varepsilon_m}{\varepsilon_s}$ following Ref(Otuka et al., 2017). was adopted to reduce the uncertainty in detector efficiency. The uncertainty in the interpolated efficiency (ε) was propagated to the efficiency ratio (η) following Section II . C of the Ref. (Ganesapandy et al., 2023). The uncertainties in t_1, t_2, t_3 in timing factor f are considered negligible. The uncertainties in λ_s and λ_m were propagated to the measured cross section. The total uncertainty (%) is the square root of the quadrature sum of the fractional

Table 3
Timing details, and γ-ray net peak counts for reaction product nuclides.

Reaction	Threshold energy (MeV)	cooling time (secs)	Counting time (secs)	γ-ray net peak counts
^{82}Se(n,2n)^{81}Se^m	9.494	1860	3671	231791 ± 539
^{80}Se(n,a)^{77}Ge	0.912	83268	3616	428 ± 50
^{78}Se(n,p)^{78}As	3.471	1860	3671	5702 ± 125
^{76}Se(n,2n)^{75}Se	11.301	83268	3616	1145 ± 85
^{76}Se(n,p)^{76}As	2.207	83268	3616	1298 ± 69
^{74}Se(n,2n)^{73}Se^g	12.22	1860	3671	6945 ± 140

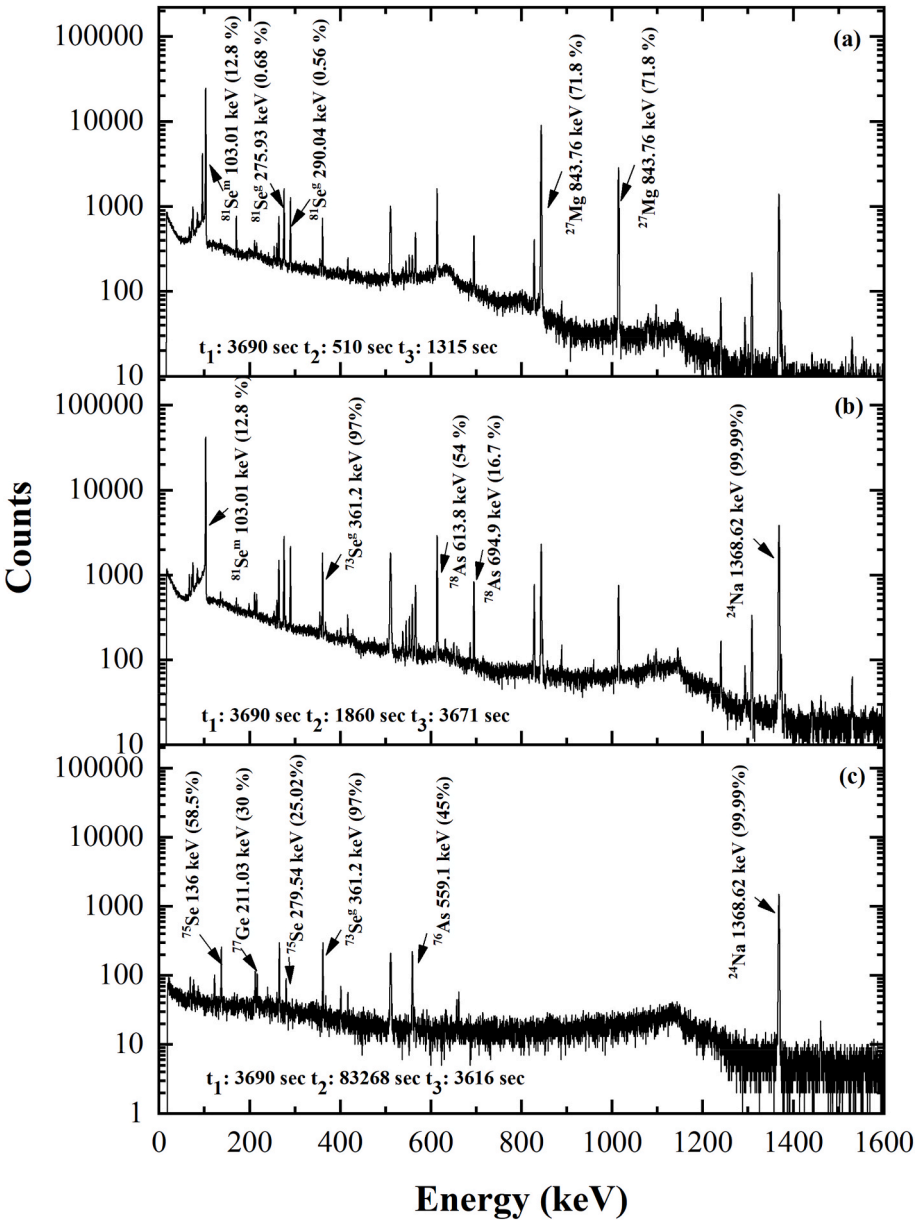

Fig. 1. Recorded γ-ray spectra for the irradiated ^{nat}Se sample and Al monitor.

Table 4
The interpolated efficiencies, correlation matrix for the product nuclides of sample, and monitor reactions.

Product Nuclide	Eγ (MeV)	ε (%)	Correlation Matrix						
$^{81}Se^{m}$	0.103	13.690 ± 0.232	1						
^{75}Se	0.136	15.251 ± 0.347	0.747	1					
^{77}Ge	0.21103	12.455 ± 0.364	0.411	0.901	1				
$^{73}Se^{g}$	0.3612	8.188 ± 0.176	0.813	0.893	0.753	1			
^{76}As	0.5591	5.679 ± 0.143	0.907	0.61	0.278	0.825	1		
^{78}As	0.6949	4.674 ± 0.112	0.926	0.678	0.349	0.837	0.988	1	
^{24}Na	1.36863	2.587 ± 0.055	0.812	0.915	0.747	0.868	0.698	0.751	1

uncertainties (%) in the parameters of **equation (1)** listed in Table 6.

3. Nuclear model calculations

The cross section of the $^{76}Se(n,2n)^{75}Se$ reaction was calculated for incident neutron energies from 13 to 17 MeV with the TALYS-1.96 (Koning et al., 2008), and the EMPIRE-3.2.3 (Herman et al., 2007) reaction codes. The contributions of compound nucleus formation, direct-like processes and pre-equilibrium processes are incorporated into these codes. The optical models viz. Wilmore-Hodgson optical model (Hodgson, 1984) and Koning-Delaroche nucleon-nucleus optical model (Koning and Duijvestijn, 2004) are valid for incident neutron energies up to 20 MeV. The transmission co-efficient for the ejectile in a nuclear reaction is determined by the optical model potential. 432 = 6 x

Table 5
Correction factor for monitor and sample product nuclides.

Product nuclide	Eγ (MeV)	Sample	*fa*	*fc*	F
$^{81}Se^{m}$	0.103	Se	1.1486	1	1.1486
^{75}Se	0.136	Se	1.0811	1.1223	1.2134
^{77}Ge	0.21103	Se	1.04	1.1614	1.2079
$^{73}Se^{g}$	0.3612	Se	1.024	1.1161	1.1429
^{76}As	0.5591	Se	1.0184	1.0142	1.0329
^{78}As	0.6949	Se	1.0175	1.046	1.0643
^{24}Na	1.36863	Al	1.0014	1.0163	1.0177

2 x 4 x 9 calculations were done with combinations corresponding to 6 level density models, 2 optical models, 4 pre-equilibrium models and 9 gamma strength functions in the TALYS-1.96 code. Chi-squared analysis of 432 calculations corresponding to the model space in the TALYS-1.96 code was done with the EXFOR data. Outlier data (Minetti and Pasquarelli, 1967; Molla et al., 1983) were not considered for Chi-squared analysis. The best reproduction of the experimental data for the $^{76}Se(n,2n)^{75}Se$ reaction was with the following combination: i) level densities calculated by Constant Temperature (Gilbert and Cameron, 1965) + Fermi Gas model (Dilg et al., 1973) ii) optical model potential for neutrons given by (Koning and Delaroche, 2003) , iii) preequilibrium model described by (Koning and Duijvestijn, 2004) and iv) Gamma strength function given by the standard Lorentzian(Axel, 1962; Brink, 1957). The uncertainty in calculated TALYS cross sections is determined by the method employed in Ref. (Ganesapandy et al., 2023). Similarly, with the EMPIRE-3.2.3 code, 168 = 4 x 2 x 3 x 7 calculations were done with combinations corresponding to 4 level density models, 2 optical models, 3 pre-equilibrium models and 7 gamma strength functions. The chosen model combination based on chi-squared analysis with the EXFOR data was i) level densities based on the microscopic HFB level densities (GORIELY et al., 2001) ii) Wilmore-Hodgson optical model iii) Monte Carlo pre-equilibrium model (Blann, 1996) and iv) Gamma strength function given by the standard Lorentzian (Brink, 1955).

4. Results and discussion

In Fig. 2, the present result is compared with the normalized literature data (Otuka et al., 2014), the statistical model calculations of TALYS-1.96 (Koning et al., 2008) and EMPIRE (Herman et al., 2007) nuclear codes for incident neutron energies from 13 to 17 MeV. The normalization of the EXFOR data is done for the reference monitor cross section data in the IRDFF-II library (Trkov et al., 2020), and gamma-ray branching ratio in the ENSDF library (Bhat, 1992). Upon normalization, the reported data of (Molla et al., 1983) changes by 10% while the change is less than 5% for the reported data of (Casanova and Sanchez, 1976; Filatenkov, 2016; Frehaut et al., 1980; He et al., 2005; Hille and Muenzer, 1966; Hoang et al., 1989; Minetti and Pasquarelli, 1967; Rao and Fink, 1967; Zhou et al., 1987). The correlation matrix for the measured neutron-induced reaction cross sections for selenium is listed in Table 7. The present result is in good agreement with the normalized data reported by Refs (Hille and Muenzer, 1966; Hoang et al., 1989; Zhou et al., 1987). within experimental uncertainty, the ENDF/B-VIII.0, and the JENDL-5 evaluations as listed in Table 8. The evaluations of TENDL-21, JENDL-5 and ENDF/B-VIII.0 are interpolated values at 14.77 ± 0.17 MeV, which is the neutron energy spread of this measurement.

5. Conclusion

The measured cross section of $^{76}Se(n,2n)^{75}Se$ reaction at 14.77 ± 0.17 neutron energy by neutron activation technique is 859.59 ± 74.44 mb. The total uncertainty in the present measurement is 8.7%. The experimental results are compared with normalized EXFOR data and evaluated data from the ENDF/B-VIII.0, JENDL-5 and TENDL-2021 libraries in Fig. 2. The measured cross section is in good agreement with the EXFOR data and the evaluated data libraries at 14.77 ± 0.17 incident neutron energy.

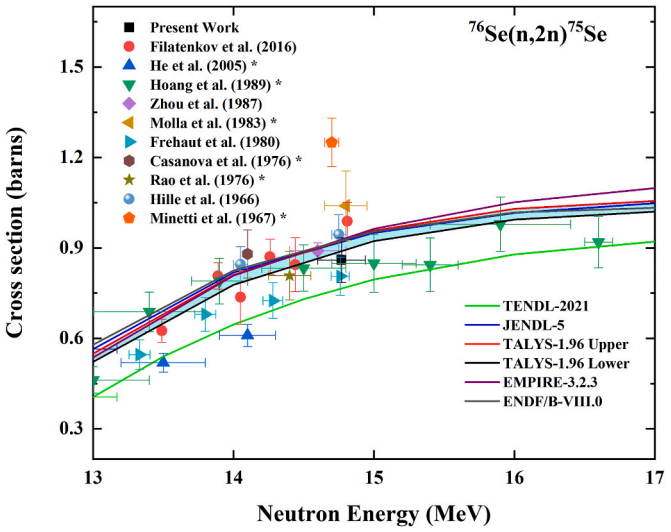

Fig. 2. Present results compared with the EXFOR data and the evaluated databases. * indicates normalization was done for the reported EXFOR data. The TENDL-2021 evaluation is denoted by a green solid line, the JENDL-5 evaluation is denoted by a blue solid line, the ENDF/B-VIII.0 evaluation is denoted by a pink solid line, the EMPIRE-3.2.3 calculations is denoted by a solid purple line, the TALYS-1.96 95% upper confidence level is denoted by a red solid line, the TALYS-1.96 95% lower confidence level is denoted by a black solid line and the region between the above two dashed lines is filled in blue.

Table 6
Partial uncertainties and for parameters and their correlation.

Nuclide Parameter	$^{81}Se^{m}$	^{77}Ge	^{78}As	^{75}Se	^{76}As	$^{73}Se^{g}$	Correlation
C_s	0.2325	11.6822	2.1922	7.4236	5.3159	2.0161	Uncorrelated
C_m	0.5861	0.8967	0.5936	0.8967	0.8967	0.5779	Fully correlated
I_{ys}	2.3438	2.6667	12.5749	0.6838	4.4444	1.0309	Uncorrelated
I_{ym}	0.0015	0.0015	0.0015	0.0015	0.0015	0.0015	Fully correlated
$\eta_{m,s}$	1.0042	1.5658	0.143	1.7532	0.246	0.4152	Partially correlated
$f_{\lambda s}$	0.0009	0.0132	0.078	0.0415	0.1243	2.0161	Uncorrelated
$f_{\lambda m}$	0.0744	0.0092	0.0745	0.0092	0.0092	0.5779	Fully correlated
M_s	0.0247	0.0247	0.0247	0.0247	0.0247	0.0247	Fully correlated
M_m	0.1752	0.1752	0.1752	0.1752	0.1752	0.1752	Fully correlated
a_s	2.52[a]	0.8264[b]	1.178[c]	3.095[d]	3.095[e]	4.4944[f]	There is a perfect correlation between **d** and **e.** However, **a**, **b**, **c,** and **f** are uncorrelated with **d** and **e**.
σ_m	2.4443	2.4443	2.4443	2.4443	2.4443	2.4443	Fully correlated
Total (%)	**4.3887**	**12.3908**	**13.0656**	**8.6626**	**8.0297**	**6.0198**	

Table 7
Correlation matrix for measured cross section with the total uncertainty for neutron-induced reactions on ^{nat}Se.

Reaction	Cross section (millibarns)	Correlation Matrix					
^{82}Se(n,2n)^{81}Se^{m}	951.26 ± 41.76	1					
^{80}Se(n,a)^{77}Ge	2.48 ± 0.31	0.131	1				
^{78}Se(n,p)^{78}As	19.13 ± 2.50	0.113	0.041	1			
^{76}Se(n,2n)^{75}Se	859.59 ± 74.44	0.206	0.086	0.059	1		
^{76}Se(n,p)^{76}As	49.72 ± 3.99	0.191	0.069	0.063	0.239	1	
^{74}Se(n,2n)^{73}Se^{g}	179.45 ± 10.80	0.254	0.094	0.082	0.137	0.136	1

Table 8
Present experimental cross section for the ^{76}Se(n,2n)^{75}Se reaction compared with evaluated data and nuclear model calculations.

Reaction	Measured cross section (millibarns)	Evaluated cross section (millibarns) at 14.77 MeV neutron energy				
		TALYS-1.96	EMPIRE-3.2.3	TENDL-2021	JENDL-5	ENDF/B-VIII.0
^{76}Se(n,2n)^{75}Se	859.59 ± 74.44	913.72 ± 17.77	934.86 ± 22.27	767.69 ± 21.98	926.68 ± 18.34	931.56 ± 18.21

CRediT author statement

T.S. Ganesapandy: Methodology; Data curation; Writing - original draft; Software; Investigation; Formal analysis; Validation.
G.T.Bholane: Validation.
S.H.Patil: Visualisation.
S.S. Dahiwale: Resources; Funding acquisition.
S.G. Kulkarni: Resources.
V.N. Bhoraskar: Conceptualization; Project administration; Supervision; Investigation.
S.D. Dhole: Funding acquisition; Project administration; Resources; Writing - review & editing; Supervision; Investigation.

Declaration of competing interest

The authors declare that they have no known competing financial interests or personal relationships that could have appeared to influence the work reported in this paper.

Data availability

Data will be made available on request.

Acknowledgement

The author [S. D. Dhole] gratefully acknowledges the financial assistance from SERB-DST, New Delhi for research work in the field of neutron induced nuclear reactions. The author [S.H.Patil] acknowledges the award of Junior Research Fellowship [File No: 09/137(12517)/2021-EMR-I] by CSIR, New Delhi.

References

Axel, P., 1962. Electric dipole ground-state transition width strength function and 7-mev photon interactions. Phys. Rev. 126, 671–683. https://doi.org/10.1103/PhysRev.126.671.
Baglin, C.M., 2008. Nuclear data sheets for A = 81. Nucl. Data Sheets 109, 2257–2437. https://doi.org/10.1016/j.nds.2008.09.001.
Bhat, M.R., 1992. In: Qaim, S.M. (Ed.), Evaluated Nuclear Structure Data File (ENSDF) BT - Nuclear Data for Science and Technology. Springer Berlin Heidelberg, Berlin, Heidelberg, pp. 817–821.
Bhoraskar, V.N., 1989. A facility for 14-MeV neutron irraddiation and activation analysis. Indian J. Pure Appl. Phys. 27, 648–655.
Blann, M., 1996. New precompound decay model. Phys. Rev. C 54, 1341–1349. https://doi.org/10.1103/PhysRevC.54.1341.
Brink, D., 1957. Individual particle and collective aspects of the nuclear photoeffect. Nucl. Phys. 4, 215–220.
Brink, D., 1955. Some Aspects of the Interaction of Light with Matter. University of Oxford.
Brown, D.A., Chadwick, M.B., Capote, R., Kahler, A.C., Trkov, A., Herman, M.W., Sonzogni, A.A., Danon, Y., Carlson, A.D., Dunn, M., Smith, D.L., Hale, G.M., Arbanas, G., Arcilla, R., Bates, C.R., Beck, B., Becker, B., Brown, F., Casperson, R.J., Conlin, J., Cullen, D.E., Descalle, M.-A., Firestone, R., Gaines, T., Guber, K.H., Hawari, A.I., Holmes, J., Johnson, T.D., Kawano, T., Kiedrowski, B.C., Koning, A.J., Kopecky, S., Leal, L., Lestone, J.P., Lubitz, C., Márquez Damián, J.I., Mattoon, C.M., McCutchan, E.A., Mughabghab, S., Navratil, P., Neudecker, D., Nobre, G.P.A., Noguere, G., Paris, M., Pigni, M.T., Plompen, A.J., Pritychenko, B., Pronyaev, V.G., Roubtsov, D., Rochman, D., Romano, P., Schillebeeckx, P., Simakov, S., Sin, M., Sirakov, I., Sleaford, B., Sobes, V., Soukhovitskii, E.S., Stetcu, I., Talou, P., Thompson, I., van der Marck, S., Welser-Sherrill, L., Wiarda, D., White, M., Wormald, J.L., Wright, R.Q., Zerkle, M., Žerovnik, G., Zhu, Y., 2018. ENDF/B-VIII.0: the 8th major release of the nuclear reaction data library with CIELO-project cross sections, New standards and thermal scattering data. Nucl. Data Sheets 148, 1–142. https://doi.org/10.1016/j.nds.2018.02.001.
Casanova, J.L., Sanchez, M.L., 1976. Measurement of the (n,p) ,(n,alpha),(n,2n) cross sections of Zn,Ga,Ge,As,and Se for 14.1 MeV neutrons, and (n,p) cross section analysis. An. Fis. 72, 186.
Dilg, W., Schantl, W., Vonach, H., Uhl, M., 1973. Level density parameters for the back-shifted fermi gas model in the mass range 40 < A < 250. Nucl. Phys. 217, 269–298. https://doi.org/10.1016/0375-9474(73)90196-6.
Farhan, A.R., Singh, B., 2009. Nuclear data sheets for A = 78. Nucl. Data Sheets 110, 1917–2080. https://doi.org/10.1016/j.nds.2009.08.001.
Filatenkov, A.A., 2016. Neutron Activation Cross Sections Measured at KRI in Neutron Energy Region 13.4–14.9 MeV, Report INDC (CCP)-0460.
Firestone, R.B., 2007. Nuclear data sheets for A = 24. Nucl. Data Sheets 108, 2319–2392. https://doi.org/10.1016/j.nds.2007.10.001.
Frehaut, J., Bertin, A., Bois, R., Jary, J., 1980. Status of (N, 2n) Cross Section Measurements at Bruyeres-Le-Chatel. INDC(USA), vol. 84.
Ganesapandy, T.S., Bholane, G.T., Patil, S.H., Dahiwale, S.S., Bhoraskar, V.N., Dhole, S. D., 2023. 14.77 MeV neutron-induced nuclear reaction cross sections for zinc, yttrium and molybdenum targets. Chin. Phys. C 47, 034002.
Ganesapandy, T.S., Bholane, G.T., Phatangare, A.B., Attar, F.M.D., Dahiwale, S.S., Suryanarayana, S.V., Bhoraskar, V.N., Dhole, S.D., 2022a. Measurements of neutron and photon induced cross sections for the production of medical isotopes of strontium. Nucl. Phys. 122445 https://doi.org/10.1016/j.nuclphysa.2022.122445.
Ganesapandy, T.S., Bholane, G.T., Phatangare, A.B., Attar, F.M.D., Dahiwale, S.S., Suryanarayana, S.V., Bhoraskar, V.N., Dhole, S.D., 2022b. Covariance analysis and measurements of photon and neutron induced nuclear reaction cross sections of gallium isotopes. Eur. Phys. J. A 137, 711. https://doi.org/10.1140/epjp/s13360-022-02918-x.
Gilbert, A., Cameron, A.G.W., 1965. A composite nuclear-level density formula with shell corrections. Can. J. Phys. 43, 1446–1496. https://doi.org/10.1139/p65-139.
Goriely, S., Tondeur, F., Pearson, J.M., 2001. A Hartree–Fock nuclear mass table. Atomic Data Nucl. Data Tables 77, 311–381. https://doi.org/10.1006/adnd.2000.0857.
He, G., Liu, Z., Luo, J., Kong, X., 2005. Cross-section measurements of (n, 2n), (n, p) and (n, a) reactions on some selenium isotopes near En=14 MeV. Indian J. Pure Appl. Phys. 43, 729–732.
Herman, M., Capote, R., Carlson, B.V., Obložinský, P., Sin, M., Trkov, A., Wienke, H., Zerkin, V., 2007. EMPIRE: nuclear reaction model code system for data evaluation. Nucl. Data Sheets 108, 2655–2715. https://doi.org/10.1016/j.nds.2007.11.003.
Hille, P., Muenzer, H., 1966. Cross-section measurements of the reactions Se-76(n,2n)Se-75, Se-74(n, p) Se-74 and As-75(n,2n)As-74 with neutron energies of about 14 MeV. Acta Phys. Austriaca 23, 44.
Hoang, H.M., Garuska, U., Marcinkowski, A., Zwiegliński, B., 1989. Cross sections of fast neutron induced reactions on selenium isotopes. Zeitschrift für Phys. A At. Nucl. 334, 285–291. https://doi.org/10.1007/BF01284556.
Hodgson, P.E., 1984. The neutron optical potential. Rep. Prog. Phys. 47, 613–654. https://doi.org/10.1088/0034-4885/47/6/001.
Iwamoto, O., Iwamoto, N., Kunieda, S., Minato, F., Nakayama, S., Abe, Y., Tsubakihara, K., Okumura, S., Ishizuka, C., Yoshida, T., Chiba, S., Otuka, N., Sublet, J.-C., Iwamoto, H., Yamamoto, K., Nagaya, Y., Tada, K., Konno, C., Matsuda, N., Yokoyama, K., Taninaka, H., Oizumi, A., Fukushima, M., Okita, S., Chiba, G., Sato, S., Ohta, M., Kwon, S., 2023. Japanese evaluated nuclear data

library version 5: JENDL-5. J. Nucl. Sci. Technol. 60, 1–60. https://doi.org/10.1080/00223131.2022.2141903.
Koning, A.J., Delaroche, J.P., 2003. Local and global nucleon optical models from 1 keV to 200 MeV. Nucl. Phys. 713, 231–310. https://doi.org/10.1016/S0375-9474(02)01321-0.
Koning, A.J., Duijvestijn, M.C., 2004. A global pre-equilibrium analysis from 7 to 200 MeV based on the optical model potential. Nucl. Phys. 744, 15–76. https://doi.org/10.1016/j.nuclphysa.2004.08.013.
Koning, A.J., Duijvestijn, M.C., Hilaire, S., 2008. TALYS-10. EDP Sciences, France.
Koning, A.J., Rochman, D., Sublet, J.-C., Dzysiuk, N., Fleming, M., van der Marck, S., 2019. TENDL: complete nuclear data library for innovative nuclear science and technology. Nucl. Data Sheets 155, 1–55. https://doi.org/10.1016/j.nds.2019.01.002.
Meija, J., Coplen, T.B., Berglund, M., Brand, W.A., De Bièvre, P., Gröning, M., Holden, N. E., Irrgeher, J., Loss, R.D., Walczyk, T., Prohaska, T., 2016. Isotopic compositions of the elements 2013 (IUPAC technical report). Pure Appl. Chem. 88, 293–306. https://doi.org/10.1515/pac-2015-0503.
Minetti, B., Pasquarelli, A., 1967. Measurements of neutron cross sections and isomeric cross section ratios in Se isotopes. Nucl. Phys. 100, 186–190. https://doi.org/10.1016/0375-9474(67)90364-8.
Molla, N.I., Islam, M.M., Rahman, M.M., Khatun, S., 1983. Measurement of Cross-Sections for Neutron Induced Reactions at 14 MeV.
Negret, A., Singh, B., 2013. Nuclear data sheets for A = 75. Nucl. Data Sheets 114, 841–1040. https://doi.org/10.1016/j.nds.2013.08.001.
Otuka, N., Dupont, E., Semkova, V., Pritychenko, B., Blokhin, A.I., Aikawa, M., Babykina, S., Bossant, M., Chen, G., Dunaeva, S., Forrest, R.A., Fukahori, T., Furutachi, N., Ganesan, S., Ge, Z., Gritzay, O.O., Herman, M., Hlavač, S., Katō, K., Lalremruata, B., Lee, Y.O., Makinaga, A., Matsumoto, K., Mikhaylyukova, M., Pikulina, G., Pronyaev, V.G., Saxena, A., Schwerer, O., Simakov, S.P., Soppera, N., Suzuki, R., Takács, S., Tao, X., Taova, S., Tárkányi, F., Varlamov, V.V., Wang, J., Yang, S.C., Zerkin, V., Zhuang, Y., 2014. Towards a more complete and accurate experimental nuclear reaction data library (EXFOR): international collaboration between nuclear reaction data centres (NRDC). Nucl. Data Sheets 120, 272–276. https://doi.org/10.1016/j.nds.2014.07.065.
Otuka, N., Lalremruata, B., Khandaker, M.U., Usman, A.R., Punte, L.R.M., 2017. Uncertainty propagation in activation cross section measurements. Radiat. Phys. Chem. 140, 502–510. https://doi.org/10.1016/j.radphyschem.2017.01.013.
Pronyaev, V.G. (Ed.), 1998. XMuDat: Photon Attenuation Data on PC Version 101 of August 1998 Summary Documentation. IAEA-NDS–195(REV.0)).
Rao, P.V., Fink, R.W., 1967. Neutron reaction cross sections of selenium and iron at 14.4 MeV. Phys. Rev. 154, 1023–1028. https://doi.org/10.1103/PhysRev.154.1023.
Shamsuzzoha Basunia, M., 2011. Nuclear data sheets for A = 27. Nucl. Data Sheets 112, 1875–1948. https://doi.org/10.1016/j.nds.2011.08.001.
Singh, B., 1995. Nuclear data sheets update for A = 76. Nucl. Data Sheets 74, 63–164. https://doi.org/10.1006/ndsh.1995.1005.
Singh, B., Chen, J., 2019. Nuclear data sheets for A=73. Nucl. Data Sheets 158, 1–257. https://doi.org/10.1016/j.nds.2019.02.006.
Singh, B., Nica, N., 2012. Nuclear data sheets for A = 77. Nucl. Data Sheets 113, 1115–1314. https://doi.org/10.1016/j.nds.2012.05.001.
Sudar, S., 2002. "TRUECOINC", A Software Utility for Calculation of the True Coincidence Correction, Iaea-Tecdoc-1275. Iaea-Tecdoc-1275. International Atomic Energy Agency (IAEA), pp. 37–48.
Trkov, A., Griffin, P.J., Simakov, S.P., Greenwood, L.R., Zolotarev, K.I., Capote, R., Aldama, D.L., Chechev, V., Destouches, C., Kahler, A.C., Konno, C., Koštál, M., Majerle, M., Malambu, E., Ohta, M., Pronyaev, V.G., Radulović, V., Sato, S., Schulc, M., Šimečková, E., Vavtar, I., Wagemans, J., White, M., Yashima, H., 2020. IRDFF-II: a New neutron metrology library. Nucl. Data Sheets 163, 1–108. https://doi.org/10.1016/j.nds.2019.12.001.
Vidmar, T., 2005. EFFTRAN—a Monte Carlo efficiency transfer code for gamma-ray spectrometry. Nucl. Instruments Methods Phys. Res. Sect. A Accel. Spectrometers, Detect. Assoc. Equip. 550, 603–608. https://doi.org/10.1016/j.nima.2005.05.055.
Weeks, K.J., Schulz, R.J., 1986. Selenium-75: a potential source for use in high-activity brachytherapy irradiators. Med. Phys. 13, 728–731. https://doi.org/10.1118/1.595838.
Zhou, M., Zhang, Y., Wang, C., 1987. Shell effect from the cross section of the (n, 2n) reaction produced by 14.6 MeV neutron. Chin. J. Nucl. Phys. 9, 34–39.